# Characterization of Synthesized $SnO_2$ Nanoparticles and its Application for the Photo Catalytic Degradation of Eosin Y in Aqueous Solution

[1]Fazal Akbar Jan*, [1]Muhammad Aamir, [2]Naimat Ullah and [1]Husaain Gulab
[1]*Department of Chemistry, Bacha Khan University Chrasadda, Khyber-Pakhtunkhwa,24420 Pakistan.*
[2]*Department of Chemistry, Qauid-i- Azam University Islamabad, 45320 Pakistan.*
fazal_akbarchem@yahoo.com*

(Received on 12th February 2020, accepted in revised form 24th August 2020)

**Summary:** The synthesized oxide ($SnO_2$) nanoparticles by sol-gel method were characterized using UV-Visible spectroscopy (UV-Vis), Fourier Transform Infrared spectroscopy (FTIR), X-rays diffraction(XRD) and Scanning electron microscopy(SEM). Using X-rays diffraction analysis different parameter were calculated such as crystallite size, d-spacing, dislocation density, number of unit cell, cell volume, morphological index, micro strain and instrumental broadening. The average particle size was 28.396 nm. Scanning electron microscopy revealed that $SnO_2$ nanopartcles are uniformly distributed. Optical properties such as band gap (energy gap = 3.6 eV) was calculated from UV-Visible spectroscopy. The characterized particles were used as photocatalyst for the degradation of Eosin dye in aqueous solution under UV light. The effect of different parameters i.e irradiation time, initial dye concentration, pH of the medium and catalyst weight on percent degradation was also studied. Mmaximum dye degradation was found at 220 minutes time interval that was 92 % using 10 ppm solution. At pH 5 the degradation of dye was found to be 94%. The catalyst dose of 0.06 g was found to be the optimum weight for the best photo catalytic degradation of Eosin Y.

**Key words:** $SnO_2$ nanoparticles, Eiosin dye, Photocatalytic, XRD, UV.

## Introduction

Adversely affected environmental processes as a result of the contamination of the physical and biological component of the earth and atmosphere system are called environmental pollution. In developed as well as developing countries environmental pollution is a global problem and due to severe long-term consequences it has attracted the attention of human beings [1]. The effluents of certain industries such as food processing, textile, cosmetics, paper, leather, plastic, pharmaceutical, dye manufacturing and printing contain various kinds of synthetic dyes. During the dyeing process about 15% of the total world production of dyes is lost and dumped to industrial effluents [1]. The complex chemical structure of dyes makes them very stable to light oxidation and biodegradability [2, 3]. Eosin Y dye is one of the dye in the effluents which belongs to xanthene dye group has a pink color and causing more serious ecological risks and environmental problems[4]. This dye has been studied to cause severe health hazards in human beings, such as liver, brain and central nervous system disorders, dysfunction of kidney and reproductive system [5, 6]. A number of techniques such as ultrafiltration, adsorption, ion exchange, reverse osmosis, chlorination, biosorption, and ozonation are in use for treatment of industrial effluents. These processes have their own merits and demerits i.e not so much cost effective for example biosorption, adsorption, filtration and ion-exchange can result in transfer of pollutant from one phase to another and lead to more serious secondary pollutants. Keeping in view the demerits of the aforementioned processes scientific community has been in the search for process to be more effective and can lead to complete degradation of toxic pollutants to non-hazardous products [7]. In order to cope with the demands of the treatment process to be environmental friendly and to overcome these problems an alternate method that is photocatalytic degradation under visible light irradiation using metal oxides such as $SnO_2$ nanoparticles has been proved effective[8]. Photocatalysts comprising of semiconductor-based materials has been developed in recent years as an alternative to organic pollutant degradation and decolourization methods [9, 10]. Belonging to an n-type semiconductor materials ($SnO_2$) has many applications in transistors, transparent electrodes, gas sensors, catalysts and batteries [11, 12]. $SnO_2$ has similarity in structure, band gap, and chemical stability to those of titanium dioxide ($TiO_2$) and thus are used photocatalyst. It has no adverse health effects when injected or inhaled $SnO_2$ because it is poorly absorbed by the human body [13]. Radiation treatment creates electron–hole pairs in semiconductor photocatalytic processes [14, 15]. $SnO_2$ nanoparticles have a wide band gap (3.6 eV at 300 K) [16]. Electrical conduction can be attributed to point defects (native and foreign atoms) which act as donors or acceptors. Faster transport of

*To whom all correspondence should be addressed.

photoexcited electrons in $SnO_2$ occur due to high electron mobility (~100–200 $cm^2 V^{-1}s^{-1}$ renders peculiar properties to $SnO_2$ and make the material useful for many applications. Their methods of preparation, electrical and optical properties have got attention of the researchers in recent years [17]. Keeping in view the hazards of the dyes in the aqueous system and importance of $SnO_2$ nanomaterials a study was designed to synthesize, characterize and apply the same for the photocatalytic degradation of Eosin Y dye in aqueous medium.

## Experimental

*Synthesis of $SnO_2$ nanoparticles*

Sol-gel method was used for the preparation of $SnO_2$ nanoparticles. All the chemicals used were analytical grade. In this typical experiment 13.38 g of Tin (IV) chloride pentahydrate ($SnCl_4.5H_2O$) was diluted in 100 mL of distilled water. To $SnCl_2$ solution 19 mL ammonium hydroxide ($NH_4OH$) was add drop wise to precipitate tin as a hydroxide and adjusting the pH of the solution to 8.2.The thick white solution (gel) formed was stirred continuously for 6 hours for the completion of the chemical reaction and the temperature was adjusted around at 70-100 $^0$C.The obtained crystalline powder was filtered and dried at 80 $^0$C for 1 hour. The dried sample was calcined for 3 hours at 600 $^0$C to get $SnO_2$ nanoparticles.

*Characterization of the nanoparticles*

UV-Visible spectrophotometer, X-Ray Diffractotmetery, Scanning Electron Microscopy and FTIR spectroscopy was used for the characterization of $SnO_2$ nanoparticles.

*Preparation of the dye solution*

The stock solution (500ppm) of Eosin Y dye was prepared by dissolving 0.125 gram of dry powder of dye in distilled water and was vigorously shaken. Different concentrations working solutions were prepared from the stock solution using dilution formula.

*Photocatalytic degradation of the dye*

For the evaluation of photocatalytic activity of $SnO_2$ nanoparticles Eosin Y dye in aqueous solution was used. For comparison the photocatalytic degradation of the dye was carried out under UV-light and sun light. The wavelength of maximum absorption of Eosin Y was 515nm and this was used as a monitor wavelength of photodegradation.

An appropriate amount of photocatalyst i.e. A $SnO_2$ nanoparticle was separately added to working solutions. For 30 min in the dark mixed solution was stirred to establish dsorption/desorption equilibrium before the photodegradation reaction. Then the dispersions were kept under light source. Experiments were carried out in locally designed equipment in which UV-lamp was placed 15 cm away from the surface of the solution. The dye degradation was checked at various intervals of times and the catalyst was removed by centrifugation. The same process was repeated under sun light irradiation. As the intensity of light is moderate in March so the experiments were performed in this month starting from 10am. The absorbance of centrifuged solution was measured *via* UV-Vissible Spectrometer. The percentage photodegradation of Eosin Y dye was calculated by using the following relation:

$$D(\%) = \frac{C_0 - C_t}{C_0} \times 100 \qquad (2)$$

where $C_0$ and $C_t$ denotes the concentrations of Eosin Y at time 0 mint and $t$ (s), respectively, and $t$ is the irradiation time.

## Results and Discussion

*XRD characterization*

XRD pattern of $SnO_2$ nanoparticles synthesized through sol-gel method are shown Fig.1. The pattern demonstrates to some extent broad and well-defined peaks and shows the crystallinity of synthesized $SnO_2$ nanoparticles. The observed pattern has prominent peaks at 2Ɵ value of 26.60°, 33.89°, 37.93°, 51.76°, 54.73°and 66.08° corresponding to (110), (101), (200), (211), (220) and (301) crystal planes respectively, well coincide with JCPDS file No. (00-021-1250) and confirms the $SnO_2$ nanoparticles formation. The $SnO_2$ shows tetragonal structure. The peaks sharpness demonstrates that $SnO_2$ nanoparticles are highly crystalline [18]. The experimental and standard diffraction angles of $SnO_2$ nanoparticle is shown in Table-1

The experimental results are in coincidence with the standard values.

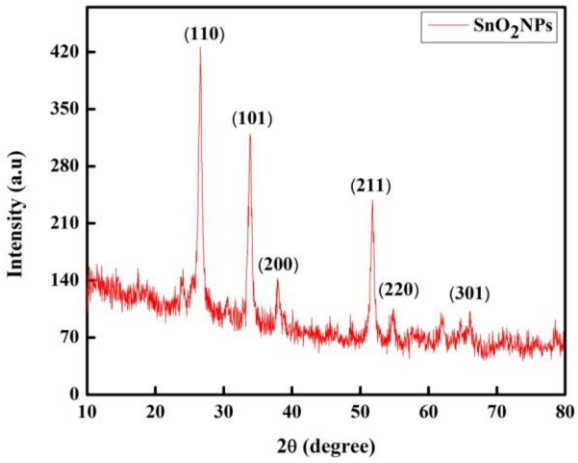


Fig. 1: XRD pattern of $SnO_2$ nanoparticles.

Table-1: Experimental and standard diffraction angle of $SnO_2$ nanoparticles.

| Experimental | Standard- JCPDS (00-021-1250) |
|---|---|
| Diffraction Angle ($2\Theta$ in degree) | Diffraction Angle ($2\ \Theta$ in degree) |
| 26.609 | 26.579 |
| 33.892 | 33.876 |
| 37.93 | 37.95 |
| 51.765 | 51.753 |
| 54.735 | 54.759 |
| 66.08 | 65.965 |

*Particle size*

The crystallite size of the $SnO_2$ nanoparticles was calculated utilizing Debye Scherrer formula as shown in equation 1

$$D = \frac{\mathbf{K\lambda}}{\boldsymbol{\beta}\cos\boldsymbol{\Theta}} \qquad (1)$$

where D is the crystallite size, $\lambda$ is the wavelength, $\beta$ is the full width at half maximum of the diffraction peak, and $\Theta$ represent Bragg diffraction angle. Using the given formula the average crystallite size was calculated to be 28.396 nm [19].

*d-spacing*

Bragg's law was used for calculating d-spacing as shown in equation 2

$$2\ d \sin\Theta = n\lambda \qquad (2)$$

$$2\ d \sin\Theta = n\lambda \qquad (3)$$

where λ is the Wavelength and value is 1.5406 Å for CuKα [20].The values d-spacing for 2Θ positions at 26.60°, 33.89°, 37.93°, 51.76°, 54.73°and 66.08° are shown in Table-2.

*Dislocation Density*

Dislocation density is characterized as the dislocation of the crystal that occurs per unit volume. Dislocation is the irregularity or crystallographic imperfection within the crystal structure or a deviation from a perfect crystal structure. Material science well explains that numerous properties are influenced due to the presence of dislocation within the crystal. The movement of one dislocation hinders the other dislocation present in crystal structure. Also, bigger the dislocation larger will be the hardness in sample. The formula for calculation of dislocation density are shown in equation 4

$$\frac{1}{D^2}^{\delta} \qquad (4)$$

where δ is the Dislocation density and D is the crystallite size of nanoparticle. The Values for dislocation density are shown in Table-2.

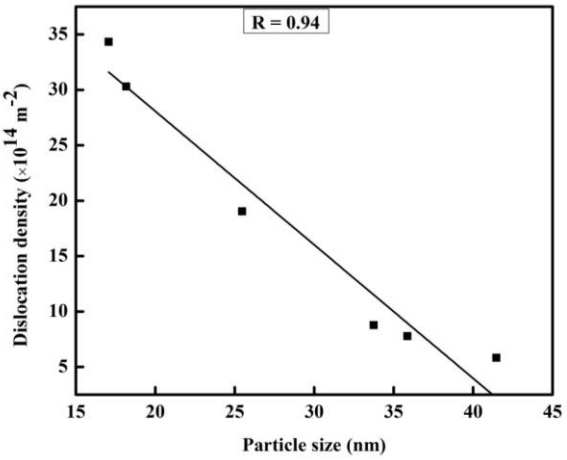


Fig. 2: Particle size Vs dislocation density curve of $SnO_2$ nanoparticles

Fig. 2 shows plot of particle size versus the dislocation density. The linear fitting of the graph shows the indirect proportion of the dislocation density with particle size as confirmed by the equation($\boldsymbol{\delta = \frac{1}{D^2}}$). This shows that by increment in the particle size the dislocation in the crystal structure is decreased.

Table-2: Diffraction angle, FWHM (β), Particle size (D), d-spacing, Dislocation density, Number of unit cell and Morphology Index of $SnO_2$ nanoparticles.

| Diffraction Angle (2Θ in degree) | FWHM(β) (Radians) | Particle Size (D) (nm) | d-Spacing (Å) | Dislocation Density ($m^{-2}$)×$10^{14}$ | Number of Unit Cell ×$10^{-31}$ | Morphological Index (Unitless) |
|---|---|---|---|---|---|---|
| 26.609 | 0.0043 | 41.464 | 3.351 | 5.816 | 5.18 | 0.714 |
| 33.892 | 0.00429 | 33.75 | 2.644 | 8.77 | 2.79 | 0.666 |
| 37.93 | 0.00858 | 17.067 | 2.369 | 34.33 | 0.3612 | 0.5 |
| 51.765 | 0.00429 | 35.87 | 1.765 | 7.77 | 3.35 | 0.666 |
| 54.735 | 0.00858 | 18.17 | 1.675 | 30.29 | 0.4358 | 0.5 |
| 66.08 | 0.00686 | 24.06 | 1.415 | 17.27 | 1.01 | 0.555 |

*Unit cells*

The number unit cells of the crystal system are calculated using the formula as given in equation 5.

$$n = \pi \left(\frac{4}{3}\right)^{x} \left(\frac{D}{2}\right)^{3x} \left(\frac{1}{V}\right) \quad (5)$$

where D is the particle size and V represent cell volume. The number of unit cell is shown in Table-2

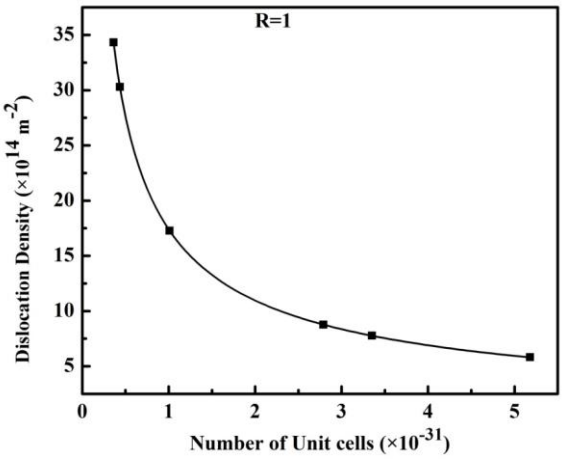


Fig. 3: Number of unit cells Vs dislocation density curve of $SnO_2$ nanoparticles.

Fig.3 shows the plot of number of unit cells versus the dislocation density. The all metrically fitted graph shows the inverse relation of number of unit cells with the dislocation density as shown by the equation $\left(n = \frac{(constant)}{\delta^{\frac{3}{2}}}\right)$. Dislocation density is a defect in which the layers of the crystals in the crystal lattice are dislocated from their original position. With increase in the number of unit cells the dislocation density of the lattice structure also decreases as shown by graphical plot and the equation.

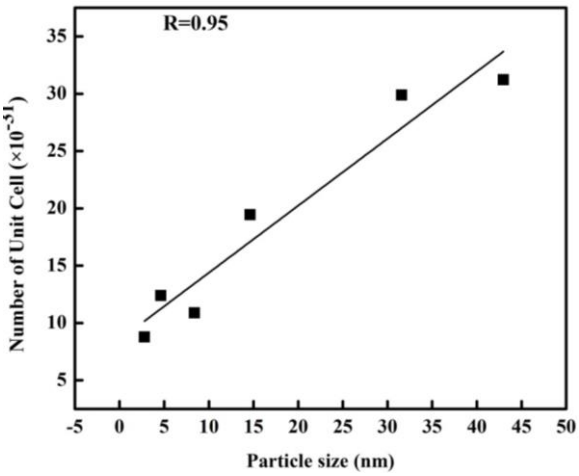


Fig. 4: Particle size Vs number of unit cells curve of $SnO_2$ nanoparticles.

Fig. 4 shows the plot of particle size versus the number of unit cells. The particle size is in direct relation with the number of unit cells as shown by the linear fit of the graph. This is also confirmed by the relation between the particle size and the number of unit cells,

$$n = \pi\left(\frac{4}{3}\right) \times \left(\frac{D}{2}\right)^{3} \times \left(\frac{1}{V}\right). \quad (5)$$

Here the number of unit cells is in direct relation with the third power of the particle size.

*Cell volume*

$SnO_2$ has tetragonal crystal symmetry [21]. Known the values of space groups the cell volume of tetragonal crystal symmetry of $SnO_2$ can be calculated from equation (6).

$$V = a^2c \quad (6)$$

where V is cell volume, a and c represent the unit cell axis dimensions. The Cell V olume of the $SnO_2$ tetragonal system was calculated to be $71.57 \times 10^{6}$ $m^{-3}$

*Morphological index*

The Morphological index for the $SnO_2$ tetragonal system is calculated from FWHM "full width at half maximum" of the XRD data. The formula for calculation of Morphological Index is given in equation (7)

$$M.I = \frac{FWHM_h}{FWHM_h + FWHM_p} \quad (7)$$

where M.I represent the Morphological Index, $FWHM_h$ shows the highest FWHM value which obtained from the peak and that of the $FWHM_p$ is the value of FWHM by which the M.I is to be calculated are given in Table-2.

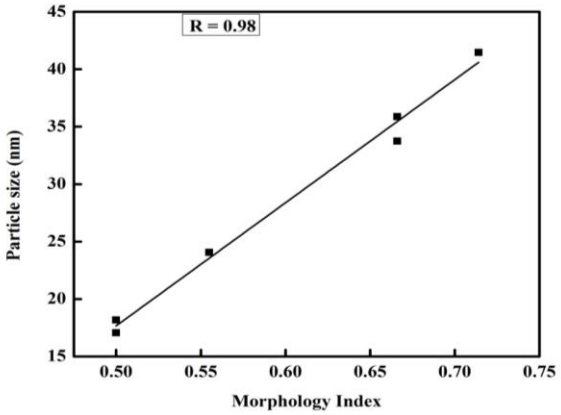


Fig. 5: Particle size Vs morphology index curve of $SnO_2$ nanoparticles.

Fig.5 shows the plot of morphological index versus the particle size of the crystal lattice. The linear fitted graph shows that on increase in the morphological index the particle size of the material also increases.

*Micro strain*

Micro strain is defined as the variation across the individual crystallite lattice parameter in term of root mean square. The Micro strain of $SnO_2$ tetragonal system are calculated by formula as shown in equation 8

$$\varepsilon = \frac{\beta}{4 \tan \Theta} \quad (8)$$

where ε is the Micro strain and $\beta$ represents the "full width at half maximum" of diffraction peaks. More ever the relationship between the Micro strain and broadening is due to micro deformation. The value of the Micro strain cannot be negative, is given in Table-3.

Table-3: FWHM (β), and Micro strain of $SnO_2$ nanoparticles.

| FWHM (Radians) | Micro Strain (Unitless) |
|---|---|
| 0.0043 | 0.00359 |
| 0.00429 | 0.00352 |
| 0.00858 | 0.00624 |
| 0.00429 | 0.00221 |
| 0.00858 | 0.004143 |
| 0.00686 | 0.002636 |

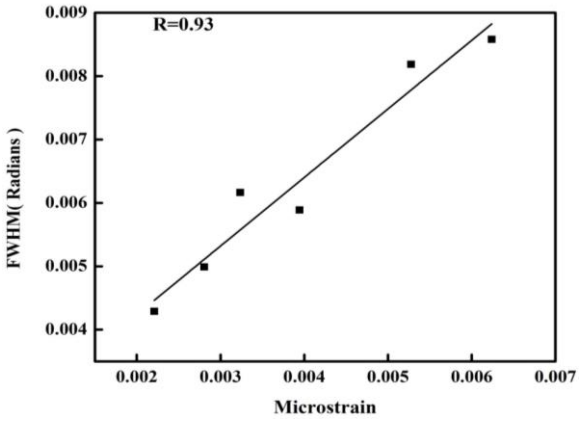


Fig. 6: Micro strain Vs particle size curve of $SnO_2$ nanoparticles.

Fig.6 shows the plot of the micro strain parameter versus the full width at half maximum. The data points show bit roughness for which we have linearly fitted the graph, which showing almost linear and direct relation between the micro strain parameter and the full width at a half maximum. Increase in full width at half maximum also increases micro strain.

*Instrumental broadening*

When particle size is less than 100 nm a substantial broadening in X-ray diffraction line will occurs. This can be attributed to the reduction of crystallite size and strain in the crystal system [22]. Both instrument and sample broadening combined to form total broadening shown by equation (11)

$$\beta^2_D = [\beta^2_{measures} - \beta^2_{Instrumental}] \quad (9)$$

$$D = \frac{K\lambda}{\beta_D \cos\Theta} \text{ Or } \cos\Theta = \frac{K\lambda}{D}\left(\frac{1}{\beta_D}\right) \quad (10)$$

$$\beta_{hkl} = \beta_s + \beta_D \quad (11)$$

where $\beta_s$ sthe sample broadening and $\beta_D$ is represent the instrumental broadening.

$$\beta_{hkl} = \left(\frac{K\lambda}{\beta_D \cos\Theta}\right) + 4\varepsilon \tan\Theta \quad (12)$$

$$\cos\Theta\ \beta_{hkl} = \left[\left(\frac{k\lambda}{\beta_D}\right) + 4\varepsilon \sin\Theta\right] \quad (13)$$

Equation (13) stands for UDM (uniform deformation model) means the strain is uniform in all crystallographic direction; ε is the micro strain of the crystal system and instrumental broadening.

Fig. 7shows the plot of the XRD peaks at 2θ position in degrees unit versus the full width at a half maximum in radians. The graph shows a rough picture of the linear and direct relation between the peaks at 2θ positions and their full width at a half maximum. For this purpose linear fitting is done with R values of 0.77 showing an almost linear and direct relation. These results showed that for peaks coming at higher 2θ values, their full width at a half maximum values also increases.

*FTIR characterization*

The Potassium bromide (KBr) pellet method was used to obtain FTIR spectrum of $SnO_2$ nanoparticles. The spectrum was taken in the range of 500-4000 $cm^{-1}$. The respective spectrum is given in fig. 8. It is clear from the spectra the successful formation of the SnO2 nanoparticles. Symmetric stretching of Sn-O-Sn occurs in the range of 500–750 $cm^{-1}$was observed.The occurance of a broad band at 651$cm^{-1}$ is the characteristic for Sn– O vibration and the band at 476$cm^{-1}$ is due the Sn–OH vibration. A characteristic of O-H stretching vibrations can be seen from a broad and weak band at 3492$cm^{-1}$

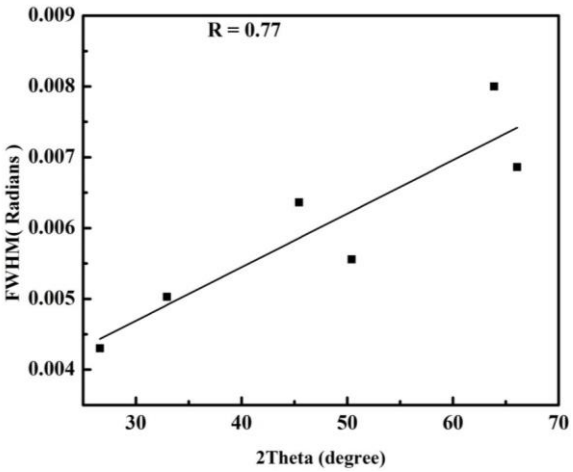


Fig. 7: Two Theta Vs FWHM curve of $SnO_2$ nanoparticles.

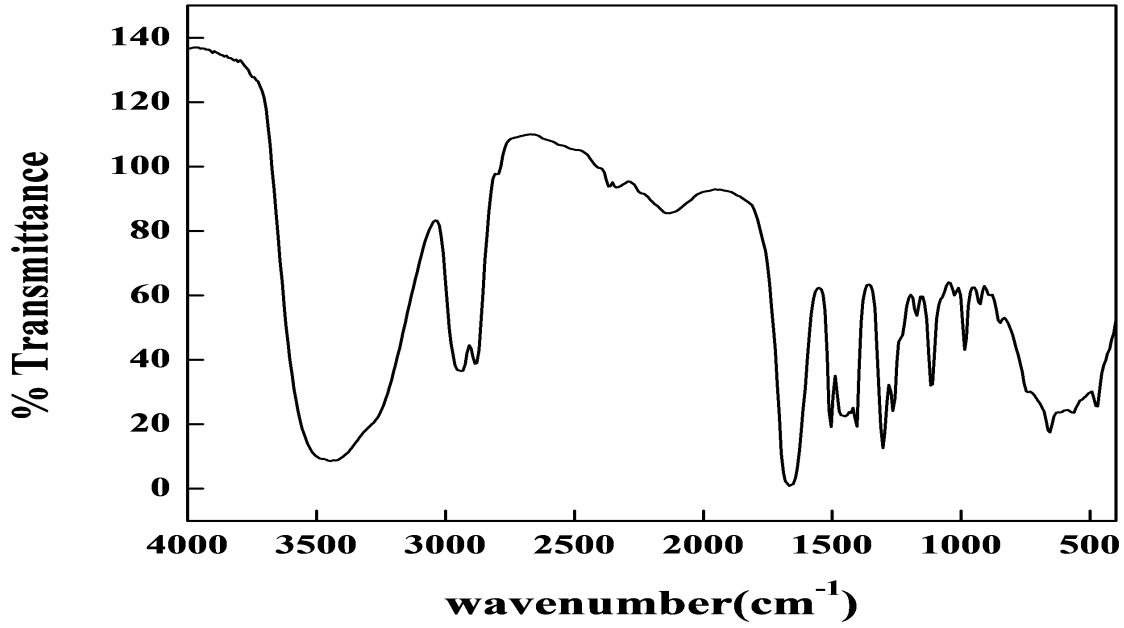


Fig. 8: FTIR spectra of $SnO_2$ nanoparticles.

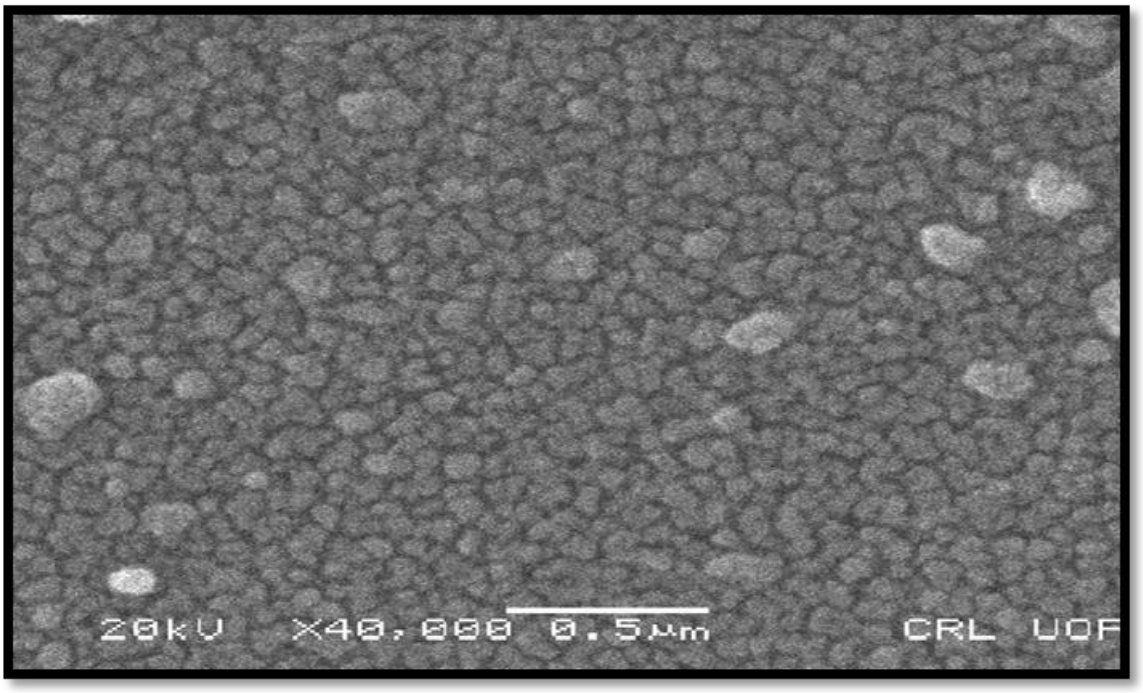


Fig. 9: Scanning electron micrograph of $SnO_2$ nanoparticles

*SEM characterization*

Fig. 9 shows the morphology of $SnO_2$ nanoparticles calcined at 600 °C. As evident from the micrograph agglomerate of particles with average diameter of less 200 nm in whole morphology. The tetragonal particle of The $SnO_2$ nanoparticles is uniformly distributed; mostly sol–gel method could be employed to synthesize the $SnO_2$ nanoparticles with fine size distribution [23].

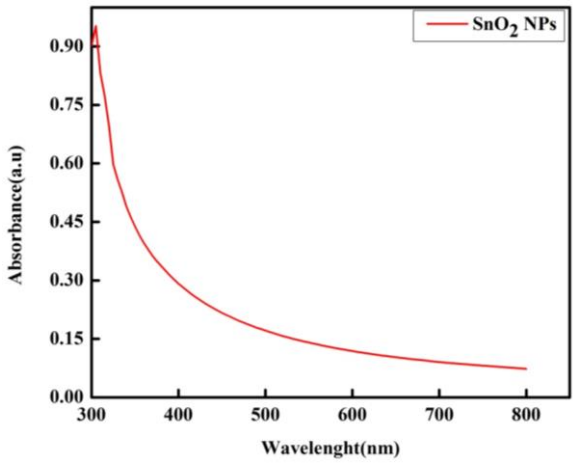


Fig. 10: UV-Visible Spectrum of $SnO_2$ NPs

*UV-visible spectroscopic characterization*

The UV-Visible spectrum of $SnO_2$ nanoparticles dispersed in ethanol is shown in Fig. 10. The spectrum shows characteristic absorption at wavelengths of 309 nm. High absorption coefficient is given in the UV region though it is transparent in the visible region [24].

*Band gap*

UV-Visible spectroscopic study was used for the calculation of band gap of $SnO_2$ nanoparticles using the equation given below [25].

$$\alpha h\upsilon = A(h\upsilon - Eg)^n \qquad (14)$$

The absorption coefficient is shown by α, photon energy by hυ and A is proportionality constant. The index is represented by n and assumes values is 1/2, 3/2, 2 and 3 depending on transition but for allowed and direct transition n = 1/2. The optical band gap of $SnO_2$ nanoparticles was calculated to be 3.6 eV, (Fig.11) which is closely related to literature value.

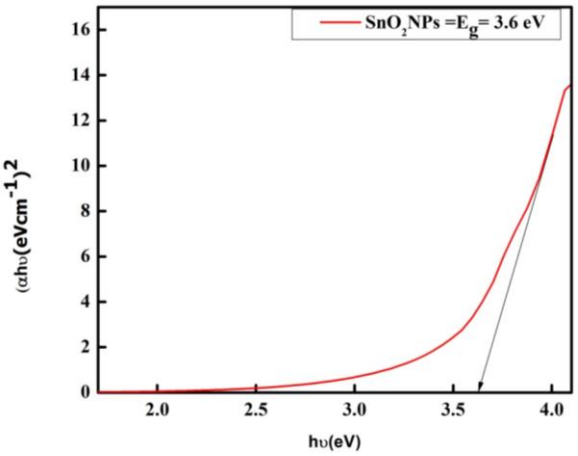


Fig. 11: Energy Gap of $SnO_2$ nanoparticles.

*Photo catalytic degradation of dye*

The activity of $SnO_2$ nanoparticles was evaluated in the photodegradation of Eosin Y dye under UV light.

Prior to illumination an optimized amount of photocatalyst was added to the dye solution. The solution was stirred in the dark for 30 minutes duration in order to reach absorption-desorption equilibrium.

In order to check the degradation efficiency (%) the solutions were analyzed using UV-Vis spectrometer. Wavelength of maximum absorption of the dye was found at 515nm [26]. Since the photocatalytic reactions are affected by various parameters therefore the effect of irradiation time, catalyst amount and pH of the solution was also studied.

*Effect of irradiation time on dye degradation*

The effect of time on the photocatalytic degradation was evaluated in terms of percentage of dye removal at different interval of time under UV light. As evident from Table-4 and Fig 12 the percent degradation enhanced from 37% - 92% with increase in time duration. Maximum photodegradation was acheived after 220 minutes of irradiation. Increase in photodegradation of the dye with increase in irradiation time can be attributed to interaction of dye molecule with the surface of the photocatalyst. Interaction of Eosin Y dye molecule with the surface of photocatalyst increases with increase in irradiation time which in turn increased the photodegradation efficiency of photocatalyst [27].

Table-4: Increase in percent degradation of the dye with increase in $SnO_2$ nanoparticles under UV light.

| Time (mints) | 20 | 40 | 60 | 80 | 100 | 120 | 140 | 160 | 180 | 200 | 220 |
|---|---|---|---|---|---|---|---|---|---|---|---|
| Degradation (%) | 37 | 49 | 57 | 61 | 60.5 | 71 | 73 | 75 | 83 | 89 | 92 |

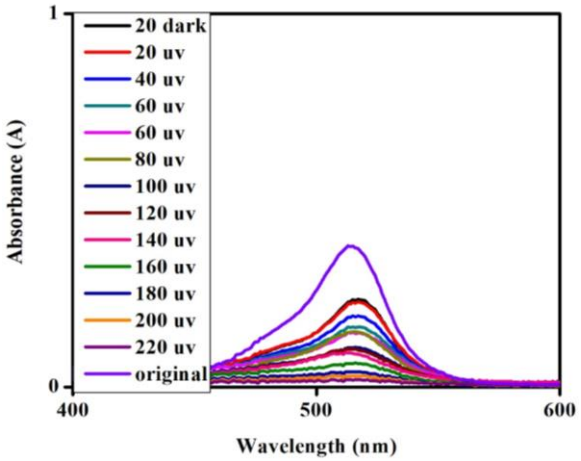


Fig. 12: Effect of time on the degradation of dye using $SnO_2$ nanoparticles under UV light.

*Effect of initial dye concentration*

A varied concentration of 10 to 50 ppm with optimum catalyst loading was taken in order to study the effect of the initial concentration of dye on degradation. As evident from Table-5 and Fig. 13 the degradation efficiency decreased with increase in the initial concentration of the dye. 90% photodegradation was achieved using low concentration (10ppm) of the dye. When the dye concentration was increased photodegradation was found to decrease. This can be attributed to the fact that the catalyst surface from light photons is shielded due to the adsorption of more dye molecules as a result of increase in the initial concentration of the dye. This is also a reason that can explain that increase in the dye concentration saturate the photo catalyst surface and the requirement of catalyst for the process also increases. Keeping the irradiation time and catalyst loading constant, the $OH^{\cdot}$ radical formation on the surface of semiconductor also become constant. That is why increasing concentration of the dye the relative number of OH• needed for the dye molecules decreases [28, 29].

Table-5**:** Decrease in percent degradation with increase in the dye concentration under UV light.

| Dye conc.(ppm) | Degradation (%) |
|---|---|
| 10 | 90 |
| 20 | 70 |
| 30 | 68 |
| 40 | 56 |
| 50 | 5 |

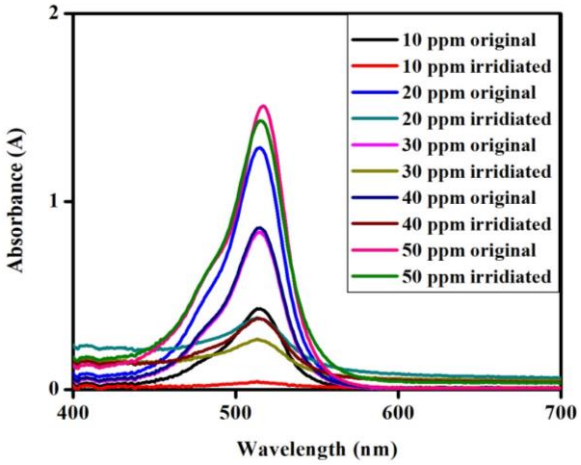


Fig. 13**:** Effect of initial concentration on the degradation of dye using $SnO_2$ nanoparticles under UV light.

*Effect of pH of the solution*

For studying the photocatalytic activity of a catalyst the pH of a solution is an important parameter because it provides valuable information about the surface charge properties of the catalyst. The effect of different pH (5, 6, 7, 8 and 9) on the degradation of Eosin Y Dye solution was also investigated. By the addition of HCl and NaOH the pH of the dye solution was varied. The percent degradation achieved using 10 ppm of Eosin Y at different pH is shown in Table-6 and fig. 14. With increase in the pH from 5 to 9 the degradation efficiency decreased. The removal efficiency decreases due to the dissolution of $SnO_2$ while going on the acidic side. pH-9 is the zero point charge of $SnO_2$. $SnO_2$ surface is almost negatively charged in aqueous solution at a pH higher than 9. Electrostatic interaction between the negatively charged $SnO_2$ surface and positively charged dye moplecules is higher in alkaline solution as a result better photodegradation is obtained [30].On other hand $SnO_2$ powder has pHpzc at about pH 5. At high pH adsorption on the catalyst surface is maximum and in turn high degradation efficiency is achieved.

Optimum degradation of Eosin Y dye was obtained at pH-5 that was 94% under the irradiation time of 220 minutes.

Table-6: Decrease in percent degradation with increase in pH of the medium under UV light

| pH value | 9 | 8 | 7 | 6 | 5 |
|---|---|---|---|---|---|
| Degradation (%) | 10 | 20 | 78 | 82 | 94 |

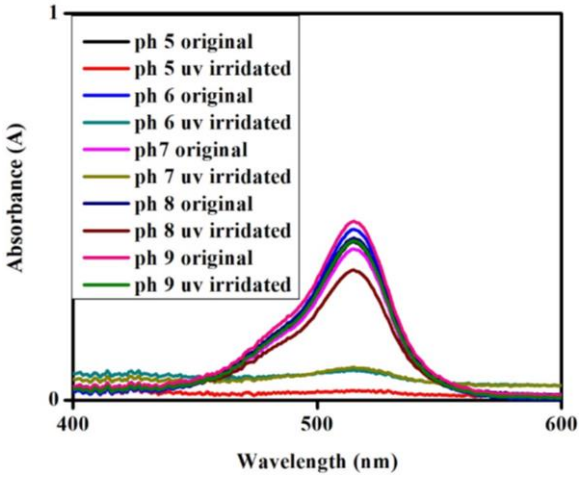


Fig. 14: Effect of pH on the degradation of dye using $SnO_2$ nanoparticles under UV light.

*Effect of catalyst dosage*

The effect of $SnO_2$ catalyst dose on the photocatalytic degradation of Eosin Y dye was evaluated using different weight ranging from 0.01 to 0.06g. The percent degradation increased with increase in catalyst weight. Maximum degradation was noticed using 0.06g of catalyst. The percent degradation using different catalyst dose in shown in Table-7 and Fig. 15. At higher catalyst dosage the OH- radical generation through catalyst active sites is higher which in turn increase in the removal of dye. Two important factors i.e. the surface area and active sites influences colour removal [31].

Table-7**:** Increase in percent degradation with increase in catalyst dose under UV light.

| Catalyst weight (g) | 0.01 | 0.02 | 0.03 | 0.04 | 0.05 | 0.06 |
|---|---|---|---|---|---|---|
| Degradation (%) | 20 | 31 | 40 | 81 | 83 | 90 |

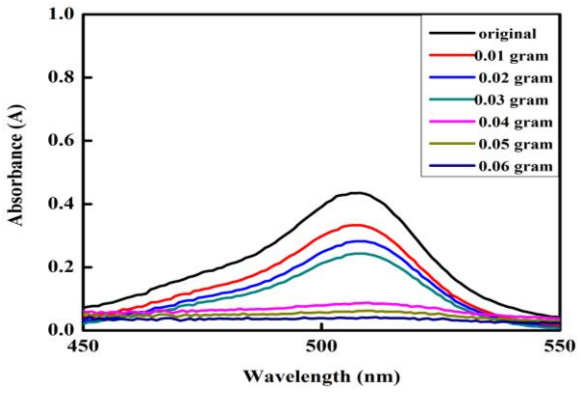


Fig. 15: Effect of catalyst dosage on the degradation of dye using $SnO_2$ nanoparticles under UV light.

## Conclusion

$SnO_2$ nanoparticles have been successfully synthesized using sol-gel technique by using the chloride penthydrate ($SnCl_4.5H_2O$) as a central precursor for the synthesis. XRD analysis revealed the average particles size is in the range of (28.396 nm). Different parameter were determined such crystallite size, d-spacing, dislocation density, number of unit cell, cell volume, morphology index, micro strain, and instrumental broadening confirmed that all these parameter are highly inter correlated. Increasing or decreasing the value of one parameter will affect other parameter. Increase of crystallite size the dislocation density decrease and hardness is also increase as a result higher value of dislocation density. It's also confirmed that number of unit cell has inverse relation to dislocation density. From morphology index calculation it was observed that there is inverse relation with crystallite size. Changing the values of 2Ɵ and FWHM leads to instrumental broadening also confirmed form plotting graph between FWHM vs 2 Ɵ. The SEM study investigate that the nanoparticles is uniformly distributed. Bending and streching frequencies of the functional groups are successfully confirmed from FTIR spectrum Optical study was conducted through UV-Visible spectroscopy as a result the band gap was calculated.

$SnO_2$ nanoparticles are suitable catalyst for the photocatalytic degradation of Eosin Y dye. Maximum degradation was found at 220 minutes time duration. The initial concentration of the dye has an adverse effect on degradation rate, due to the anionic nature of the dye. Lower pH improved the catalyst efficiency. With increase in catalyst weight the rate of degradation of the dye increases

## References


1 H. Zollinger, *Color chemistry: syntheses, properties, and applications of organic dyes and pigments*, John Wiley &Sons (2003).

2 A. E. Ofomaja and YS *Bioresour*, Effect of temperatures and pH on methyl violet biosorption by Mansonia wood sawdust. *Technol.*, **99**, 5411(2008).

3 Z. Aksu, Application of biosorption for the removal of organic pollutants: a review. *Process Biochem.*, 40997(2005).

4 D. E. Tanasa,C. G. Piuleac, S. Curteanu and E Popovici, Photodegradation process of Eosin Y using ZnO/SnO 2 nanocomposites as photocatalysts: experimental study and neural network modeling. *J. Mater. Sci.* **48,** 8029 (2013).

5 Z. Ajji and A. M. Ali, Adsorption of methyl violet and brilliant blue onto poly (vinyl alcohol) membranes grafted with N-vinyl imidazole/acrylic acid. *Nucl.Instrum. Methods Phys. Res.***265**, 362 (2007).

6 K.Kadirvelu,M. Kavipriya,C. Karthika, M. Radhika,N.Vennilamani and S Pattabhi, Utilization of various agricultural wastes for activated carbon preparation and application for the removal of dyes and metal ions from aqueous solutions. *Bioresour.Technol.*, **87,** 129 (2003).

7 A. P. Rao, A. M. Umabala and P Suresh, Visible light assisted photo catalytic degradation of 2, 4-dinitrophenol and 2, 4, 6-trinitrophenol using $H_2O_2$ sensitized BiVO4.*Appl. Chem.*, **4**, 1145(2015).

8 S. P. Kim,M. Y. Choi and H. C. Choi, Use of lactic acid modified MoS2 nanopetals to improve photocatalytic degradation of organic pollutants. *Mater.Res. Bullet.*,**74,** 85( 2016).

9 K. Sayama, H. Hayashi,T. Arai,M.Y.anagida,T. Gunji and H Sugihara, Highly active WO3 semiconductor photocatalyst prepared from amorphous peroxo-tungstic acid for the degradation of various organic compounds. *Appl. Catal. B-Environ.*, **94**, 150(2010).

10 J. Hirayama,H. Kondo,Y.K. Miura,R. Abe and Y.Kamiya, Highly effective photocatalytic system comprising semiconductor photocatalyst and supported bimetallic non-photocatalyst for selective reduction of nitrate to nitrogen in *water.Catal. Commun*., **20**, 99 (2012).

11 T. Kimura,Y. Yamauchi and N. Miyamoto, Condensation and Crystallinity Controlled Synthesis of Titanium Oxide Films with Assessed Mesopores. *Chem. Eur. J*., **16**, 12069 (2010).

12 H. Wang, F. Fu, F. Zhang, H. E. Wang, S.V.Kershaw, J. Xu, S.G. Sun and A. L. Rogach, Hydrothermal synthesis of hierarchical SnO 2 microspheres for gas sensing and lithium-ion batteries applications: Fluoride-mediated formation of solid and hollow structures .*J. Mater. Chem.*, **22**, 2140 (2012).

13 A. Bhattacharjee, M. Ahmaruzzaman and T.Sinha, *Acta A-Mol. Biomol. Spectrosc*. **136**, 751 (2015).

14 S.C.Yeow,W.L. Ong,A.S.W. Wong and G.W.Ho,Template-free synthesis and gas sensing properties of well-controlled porous tin oxide nanospheres. *Actuators B-Chem.*, **143**, 295 (2009).

15 H. Yuan and J. Xu, Incorporation of graphenes in nanostructured TiO2 films via molecular grafting for dye-sensitized solar cell application. *Int. J. Chem. Eng. Appl*., **1**, 241 (2010).
16 G. Suresh, R.Sathishkumar, B. Iruson, B. Sathyaseelan, K. Senthilnathan and E. Manikandan, Study on structural, luminescence properties and Hall Effect of SnO2 nanoparticles obtained by a Co-precipitation technique. *Inter. J Nano Dim*., **10**, 242 (2019).
17 G. Sanon, R. Rup and A.Mansingh,Promotion of acceptor formation in SnO 2 nanowires by e-beam bombardment and impacts to sensor application. *Phy. Rev.B.,* **144**, 5672 (1991).
18 A. R. Bushroa, R. Rahbari, H. H. Masjuki and M. R. Muhammad, Approximation of crystallite size and microstrain via XRD line broadening analysis in TiSiN thin films. *Vacuum* **86**, 1107 (2012).
19 D. Patil, P. Patil, Y. K. Seo and Y. K. Hwang, Poly (o-anisidine)–tin oxide nanocomposite: synthesis, characterization and application to humidity sensing. *Sensors and Actuat* B- *Chem.*, **148**, 41 (2010).
20 Z. Luo, Y. Zhu, E. Liu,T. Hu, Z. Li and T. Liu, Revitalizing carbon supercapacitor electrodes with hierarchical porous structures. *Mater. Res. Bullet*., **60**, 105 (22017).
21 P. Bhattacharya,S. Dhibar, G. Hatui, A. Mandal,T. Das and C. K. Das, Graphene decorated with hexagonal shaped M-type ferrite and polyaniline wrapper: a potential candidate for electromagnetic wave absorbing and energy storage device applications. *RSC Advances* **41**, 7039 (2014).
22 A. N. Naje, A. S. Norry and A. MSuhail, Influence of lanthanum precursors on the heterogeneous La/SnO 2–TiO 2 nanocatalyst with enhanced catalytic activity under visible light. *Int. J. Innov. Res. Sci. Eng. Technol.*, 27068 (2013).
23 C. Ramli, Z. Amali, N. Asim, W. N. Isahak, Z. Emdadi, N. Ahmad-Ludin and K. Sopian, Photocatalytic Degradation of Methylene Blue under UV Light Irradiation on Prepared Carbonaceous. *The Sci. World J*., (2014).
24 S. Sheng Pan, S. Fung Yu,Y.X. Zhang and Y.Y.Luo, Crystallite size-modulated exciton emission in SnO2 nanocrystalline films grown by sputtering. *J Appl. Physics*, **113**, 143104 (2013).
25 W. Baran, A. Makowski and W. Wardas, The influence of $FeCl_3$ on the photocatalytic degradation of dissolved azo dyes in aqueous TiO2 suspensions, *Chemosphere*, **53**, 87 (2003).
26 K. M. Reza, A. S. W.Kurny and F.Gulshan,Parameters affecting the photocatalytic degradation of dyes using TiO 2: a review. *Appl.Water Sci*., **7**, 1569 (2017).
27 A. Salama, A. Mohamed, N. M. Aboamera,T. A. Osman and A. Khattab, Photocatalytic degradation of organic dyes using composite nanofibers under UV irradiation. *Appl. Nanosci*., **8**, 155 (2018).
28 N. Daneshvar, D. Salari, A. R. Khataee, Photocatalytic degradation of azo dye acid red 14 in water: investigation of the effect of operational parameters. *J Chem. Technol. Biotechnol*., **157**, 111 (2003).
29 E. M. Saggioro, A. S. Oliveira, T. Pavesi, C. G. Maia, L. F. V. Ferreira J. C. Moreira, Use of titanium dioxide photocatalysis on the remediation of model textile wastewaters containing azo dyes. *Molecules*, **16**, 10370 (2011).
30 N. Pugazhenthiran, P. Sathishkumar, S. Murugesan and S. Anandan, Effective degradation of acid orange 10 by catalytic ozonation in the presence of Au-Bi2O3 nanoparticles. *Chem. Eng. Jour.*, **168**, 1227 (2011).
31 S. Shokrollahzadeh and M. Abassi, A new nano-ZnO/perlite as an efficient catalyst for catalytic ozonation of azo dye. *Environ. Eng. Res*., **24**, 513 (2018).